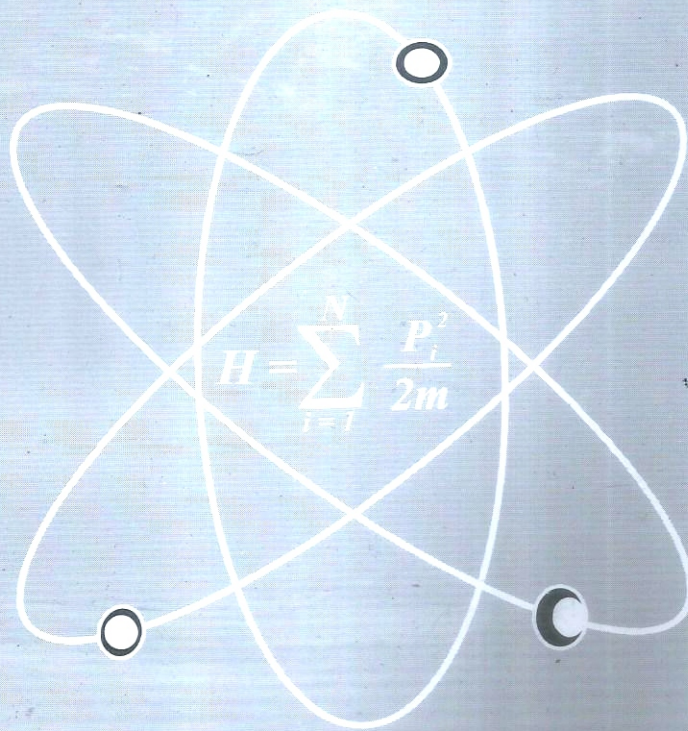


# **BAYERO JOURNAL OF PHYSICS AND MATHEMATICAL SCIENCES**



**VOLUME 9, No. 1  
JULY, 2018.**

**Published by:  
THE DEPARTMENTS OF PHYSICS AND  
MATHEMATICAL SCIENCES, BAYERO UNIVERSITY, KANO.**



## MEMBERS OF THE EDITORIAL BOARD

<b>Editor in Chief:</b>	- Prof. A. O. Musa, Dept. of Physics, Bayero University, Kano.
<b>Asst. Editor-in-Chief 1</b>	- Prof. U. M. Gana, Dept. of Physics, Bayero University, Kano.
<b>Asst. Editor-in-Chief 2</b>	- Prof. Bashir Ali, Dept. of Mathematical Sciences, B.U.K., Kano.
<b>Circulation Editor</b>	- Prof. Garba Babaji.
<b>Business Editor</b>	- Prof. F. S. Koki
<b>Secretary</b>	- Mal. Usman Muhammad. Ibrahim

## MEMBERS OF THE BOARD OF TRUSTEE

1. The Head of the Department of Mathematics Sciences, Bayero University, Kano.
2. The Head of Physics Department, Bayero University, Kano.
3. Members of the Editorial Board.

## MEMBERS OF THE EDITORIAL ADVISORY COMMITTEE

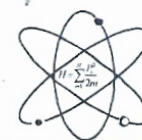
1. Prof. I. H. Umar, Department of Physics, Bayero University, Kano.
2. Prof. M. Y. Bello, Department of Computer Science, Bayero University Kano.
3. Prof. A. S. Sambo, former Director-General, National Energy Commission of Nigeria, Abuja.
4. Prof. E. U. Utah, Department of Physics, University of Uyo, Akwa Ibom State.
5. Prof. B. Osazuwa, formerly of Department of Physics, Ahmadu Bello University, Zaria.
6. Prof. J. Katande, Dean at Botswana International University of Science and Technology.
7. Prof. P.N. Okeke, Department of Physics and Astronomy, University of Nigeria, Nsukka.
8. Prof. M. N. Agwu, Department of Physics, Nigerian Defence Academy, Kaduna.
9. Prof. Ado. Dan-Isa, Department of Electrical Engineering, Bayero University, Kano.
10. Dr. M. S. Abubakar, Department of Physics, Kaduna State University, Kaduna.
11. Dr. B. S. Galadanchi, Department of Electrical Engineering, Bayero University, Kano.
12. Prof. M. B. Yakasai, Department of Mathematics Sciences, Bayero University, Kano.
13. Dr. N. F. Isa, Department of Physics, Bayero University, Kano.
14. Prof. Garba Uba Goje, Dept. of Mathematical Sciences, Ahmadu Bello University, Zaria.
15. Prof. Babangida Sani, Dept. of Mathematical Sciences, Ahmadu Bello University, Zaria.



## TABLE OF CONTENTS

Preparation of Microspherical Flowerlike Ni(OH) <sub>2</sub> /Graphene Oxide Electrode for Electrochemical Capacitor Application <b>Khaleed, A. A., Igumbor, E. and Omotoso, E.</b>	1 – 8
Parabolic Trough Solar Collector: Development and Performance Evaluation Using Selected Absorber Coatings <b>Yunusa, A. and Abusafiyan, A.</b>	9 – 15
Electronic Transport Properties of Vinazene Molecular Device for Photovoltaic Applications By Dft-Negf Approach <b>Lawal, A. Ebea Moses, A. and Gidado, A. S.</b>	16 – 24
Physicochemical Analysis of Water Samples of Selected Borehole from some Local Government in Kano, Kano State, Nigeria. <b>Auwalu, S., Usman, Y. K., Lawan, I. and Farouq, S. M.</b>	25 – 34
Design and Construction of Microcontroller Based Automatic Car Parking System. <b>Galadanci, G. S. M. and Galadima, B. Y.</b>	35 – 48
Total Reaction Cross Section and One-Nucleon Removal Cross Section of <sup>37</sup> Mg from <sup>37</sup> Mg + <sup>12</sup> C → <sup>12</sup> C + <sup>36</sup> Mg + <sup>1</sup> n Reaction System in the Glauber Theorem <b>Adamu, I. D. and Sa'adu, I.</b>	49 – 54
Calculation of Reactions Cross-Section by Particles Induced Nuclear Reactions <b>Ahmad, I., Koki, F. S., and Ibrahim, Y. Y.</b>	55 – 63
First Principle Study of Thermodynamic and Optical Properties of Tm <sup>3+</sup> Interstitial in Germanium, Using Hybrid Functional (HSE06). <b>Igumbor, E., Khaleed, A. A. and Omotoso, E.</b>	64 – 68
Evaluation of Air Pollutants and the Effect of its Transport and Mixing Processes on Air Quality: A Case Study of Selected Industries in Kano State - Nigeria. <b>Idris, M., Darma, T. H., Koki, F. S. and Said, R. S.</b>	69 – 78
Synthesis, Structural and Electrical Properties of Nanocrystalline Barium Titanate Ceramic Using Mechanochemical Method. <b>Muazu, A., Ahmadu, U., Umar, S., Amoka, A.</b>	79 – 88
Theoretical Analysis of the Exponentiated Generalized U-Quadratic Distribution <b>Muhammad, M., Rano, S. A., Sani, R. I. and Musa, S. A.</b>	89 – 100
Spotlighting the Geophysical Modeling <b>Saleh, M.</b>	101 – 108
Electronicstructure Properties Analysis of Zinc Oxide Nanosheets Attached to in Electrodes. <b>Yusuf, S., Tarauni, Y. U., Abdullahi, S. S., Muhammad, A., Ali, M. U., Aliyu, A. and Jamo, H. U.</b>	109 – 118
Application of Electrical Resistivity Method for Investigation of Competence of Building Foundation at the Permanent Site of Yusuf Maitama Sule University Kano, Nigeria. <b>Yusuf, S. and Aku, M. O.</b>	119 – 126
A Review on a Study of Farm and Soil Pollution Using Magnetic Susceptibility Method <b>Zira, A. M., Lawal, A. A. and Sule, P.</b>	127 – 135
Magnetic Susceptibility of Irrigation Farm Soil as a Proxy for Pollution Study <b>Aminu, A. L., Sule P. and Zira, A. M.</b>	136 – 144
Single Crystal Silicon Solar Cells – A Review <b>Musa, A. O. and Yunusa, A.</b>	145 – 153
Structural Performance of Bismuth Oxide Doped Zinc Silicate (Willemite) Glass Ceramics from Waste Material <b>Auwalu, I. A., Jamo, U. H., Diso, D. G., Aminu, A., Inuwa, A. F., Alhassan, M. and Umar, S. A.</b>	154 – 159
Enhancing Mechanical Properties of Porcelain Body By Substituting Quartz by RHA at Different Mould Pressures <b>Jamo, U. H., Abdu, S., Ibrahim, K. L., Muhammad, A., and Yusuf, H.</b>	160 – 168
Geomagnetic Evaluation of the Basement Structure at the Permanent Site of Federal University Lokoja, Kogi State <b>Gani, L. I., Ibrahim, A. and Rabba, J. A.</b>	169 – 178
Evaluation of Essential and Toxic Elements in Date Palm Fruits around Zaria area using Atomic Absorption Spectrometry <b>Onoja, M. A., Kassimu, A. A., David, D. and Umar, J. L.</b>	179 – 183
First Principles Study of Electronic, Elastic and Optical Properties of Bi <sub>2</sub> Te <sub>3</sub> under Pressure <b>Lawal, A., Kona, A. M. and Madugu, M. L.</b>	184 – 197
Model Predictive Control Design For Magnetic Suspension System <b>Gaya, M. S., Abdulkadir, R. A., Muhammad, A., Saleh, M. A., Umar, I. D. and Imam, K. A.</b>	198 – 202
Evaluation of Excitation Function for the Productions of Polonium-207 and Polonium-208 Isotopes from Bismuth-208 Nucleus <b>Ahmad, I.</b>	203 – 209
Impedance and Modulus Spectroscopy Studies on Lead Free Ba (Ti <sub>0.96</sub> Sn <sub>0.02</sub> Zr <sub>0.02</sub> ) O <sub>3</sub> Ceramics <b>Muazu, A., Ahmadu, U., Halim, A., Umar, S. and Amoka, A.</b>	210 – 224
Neutron Removal Cross Section From Elastic and Inelastic Breakup Processes of <sup>11</sup> Be From <sup>11</sup> Be + <sup>12</sup> C → <sup>12</sup> C + <sup>10</sup> Be + <sup>1</sup> n Reaction System <b>Adamu, I. D. and Sa'adu, I.</b>	225 – 230
Magnetic Properties of Nano-structured CoCrTa thin films <b>Gana, U. M.</b>	231 – 235
Remanence Properties of Nano-structured CoCrTa thin films <b>Gana, U. M.</b>	236 – 240
Spectral Analysis of High Aeromagnetic Data Over Kobo. (Sheet Number 80), Kano State, Nigeria <b>Suleiman, A., Aku, M. O. and Sanusi, Y. A.</b>	241 – 248
Analysis of Heavy Metals Accumulation and Sources / Origin in Fish (Tilapia) Organs using Statistical Tools <b>Isa, N. F., Haladu, B., Tijjani, B. I. and Ibrahim, M. U.</b>	249 – 256





## SYNTHESIS, STRUCTURAL AND ELECTRICAL PROPERTIES OF NANOCRYSTALLINE BARIUM TITANATE CERAMIC USING MECHANOCHEMICAL METHOD.

Muazu, A.<sup>1\*</sup>, Ahmadu, U.<sup>2</sup>, Umar, S.<sup>3</sup>, Amoka, A.<sup>3</sup>,

<sup>1</sup>Department of Physics, Federal College of Education (T), Bichi, Kano, Nigeria.

<sup>2</sup>Department of Physics, Federal University of Technology, P.M.B. 65, Minna, Nigeria.

<sup>3</sup>Department of Physics, Ahmadu Bello University, Zaria, Nigeria.

\*Corresponding author.

E-mail address: hasumm@yahoo.com

### Abstract.

Barium Titanate ( $BaTiO_3$  or BT) powders were synthesized by a combination of solid state and mechanochemical method. The thermal decomposition, phase formation, microstructure and electrical behavior were investigated by TG-DSC analysis, X-ray diffraction, FE-SEM measurements and Impedance Analyzer. The X-ray diffraction patterns show cubic symmetry without secondary phase. The lattice parameter  $a$ ,  $c/a$  ratio and crystal size was found to be  $4.0070 \text{ \AA}$ , 1.0000 and 31.2 nm. The FE-SEM results indicated dense microstructure with an average grain size of 144.53 nm. The dielectric constant and loss of BT at room temperature were 1600 and 0.77 at 40 Hz. The temperature dependence of dielectric permittivity shows that phase transition seems to be shifted towards lower room temperature with  $T_c$  observed at  $90^\circ\text{C}$ . The hysteresis loop was observed having a remanent polarization ( $P_r$ ) and coercive field ( $E_c$ ) of  $0.27 P_r (\mu\text{C}/\text{cm}^2)$  and  $581.73 E_c (\text{V}/\text{cm})$ . The dielectric constants and relatively lower loss tangent values meet the current demand for device miniaturization in the electronics industry.

**Keywords:** Barium Titanate ceramics; high energy ball milling; XRD; FESEM; dielectric properties; ferroelectricity

### 1.0 Introduction.

Barium titanate ( $BaTiO_3$  or BT) is one of the most basic and widely applied ferroelectric oxide materials with a perovskite-  $ABO_3$  type crystalline structure. It is chemically and mechanically remarkably stable, and it exhibits ferroelectric properties in and above room temperature (RT). It can easily be prepared and used in the form of ceramic polycrystalline samples [1]. Due to its excellent dielectric, ferroelectric, piezoelectric, pyroelectric and optoelectric properties [2, 3], it is extensively used in multilayer ceramic capacitors (MLCC), a positive temperature coefficient of resistance (PTCR) thermistors, piezoelectric sensors, actuators and ferroelectric random access memories (FRAM) and electro-optic devices [4, 5]. There is existing demand for fabrication of fine particle, nanosized powders  $<100 \text{ nm}$  to allow the production of thinner layers for MLC-s and cheaper or more reliable routes than current practice. BT nano-powders can be obtained via several routes among which: including coprecipitation [6], hydrothermal synthesis [7], sol-gel synthesis [8], alkoxide hydrolysis [9], citrate routes [10], and ultrasonic spray-pyrolysis [11] and mechanical synthesis [12] are the most important ones.

Mechanochemical activation technique is one of the most outstanding processes for the synthesis of advanced materials and is closely related to different structural changes such as phase transitions, generations of strains, dislocation, crystal lattice deformation or morph structural modifications, all brought about by mechanical energy involved in the milling process. In the case of conventional solid state reaction, the phases formed at the reactant



surfaces growth by diffusion of thermally activated atoms through the interfaces and this mass transport needs high temperatures and high energy consumption in order to complete the reaction and formation of the compound. In the case of intensive milling, the contact area between the reactant particles increases by continuous particle comminuting, thus creating new fresh surfaces through which the diffusion and mass transport take place easier. Moreover, the particles undergo a mechanical treatment by which the impact energy may become comparable to the energy of the crystal lattice thus allowing an easier movement of the atoms involved in the formation of the new phases.

Therefore one can assume that the fine and ultrafine powders become mechanically activated and the chemical reactions between them are stimulated to take place at lower temperature during mechanochemical synthesis without any extra heat. Unfortunately, the nature of this extremely high activity is not yet fully understood and efforts are made by the scientific community to go deeper in the understanding of this phenomenon. This paper reports on powder synthesis, structural and electrical properties of Barium titanate sintered samples obtained from solid state and mechanochemical method. The thermal decomposition, crystallinity, microstructure and electrical properties are respectively, investigated by TG-DSC analysis, X-ray diffraction (XRD), FESEM and impedance analyzer measurements.

## 2.0 Materials and Method

### 2.1 Synthesis of Barium titanate (BT)

Barium titanate (BT) was prepared from high-purity (99.9%) analytical reagent (AR) grade of  $\text{BaCO}_3$  and  $\text{TiO}_2$ . Stoichiometric amounts of the oxides were weighed according to nominal composition and ball-mixed for 12 hrs. in alcohol. The slurry was dried in an oven at  $90^\circ\text{C}$  for 24 hrs and calcined in an alumina crucible at  $1050^\circ\text{C}$  for 4 hrs. in the air to yield  $\text{BaTiO}_3$  Powder. 5g of the calcined powders were ball milled in an isopropyl alcohol as wetting medium using SPEX 8000 Mixer/Mills functionally described as shaker mills or high-energy ball mills, the Mixer/Mills shake containers back and forth approximately 1080 cycles per minute (60 Hz model) with was carried out at room temperature for 7 hrs. The milling was stopped for 15 min after every 60 minutes of milling to cool down the system. The slurry was put in an oven and dried at  $90^\circ\text{C}$  for 24 hrs. The milled powder was compacted at 5 Ton to make pellets of size 10 mm in diameter and 1 mm in thickness using polyvinyl alcohol (PVA) as a binder. After burning off the binder (PVA), the pellets were sintered in a programmable furnace at temperatures of  $1190^\circ\text{C}$  for 2hr in alumina crucibles.

### 2.2 Characterization

The DSC and TG analysis of the BT sample was carried out using differential scanning calorimetric and thermogravimetric analysis by heating the sample from  $30^\circ\text{C}$  to  $1200^\circ\text{C}$ . TG-DSC curves were recorded with a thermo analyzer Brand Metler Toledo, Model number TGA/DSC HT. The heating was carried out in air from room temperature to  $1200^\circ\text{C}$  at a heating rate of  $10\text{k}/\text{min}$ , using  $\alpha\text{-Al}_2\text{O}_3$  as a reference. Phase identification of calcined and sintered powders was identified by using X-ray diffractometer with monochromatic  $\text{CuK}\alpha$  radiation ( $\lambda = 1.54178 \text{ \AA}$ ) under  $40\text{kV}/30\text{mA}$ - over a  $2\theta$  angle from  $20^\circ$  to  $80^\circ$  at a scanning rate of 2 degrees per min. The experimental density of the samples was calculated using Electronic Densimeter MD-3005 ALFAMIRAGE. The Experimental densities ( $\rho_{exp}$ ) of the mechanochemically sintered BT ceramics were measured using Archimedes' principle [13].

$$\rho_{exp} = \frac{M_a \rho_w}{M_a - M_w} \quad (1)$$

Where  $M_a$  and  $M_w$  are respectively the weight in gram of the pellet measured in air and in water. Theoretical density ( $\rho_{th}$ ) of the sample was calculated from the molecular weight of the samples and its lattice parameter.



$$\rho_{th} = \frac{Z.M.u}{V} \tag{2}$$

were  $Z$  is the number of atom per unit cell,  $M$  is the molar mass of the composition in g/mol,  $u$  the atomic mass unit of  $1.66057 \cdot 10^{-27}$  kg and  $V$  the volume of the unit cell in  $\text{g/m}^3$ . The percentage porosity was calculated using the formula:

$$\% \text{ porosity} = \frac{(\rho_{th} - \rho_{exp})}{\rho_{th}} \times 100 \tag{3}$$

The morphological studies of the sintered sample were carried out using field emission scanning electron microscopy (FE-SEM) (JEOL 7600F) operated at 15kV. The average crystallite size  $t$  of BT ceramic was calculated from the full width at half maximum of the (110) diffraction peaks using Scherer formula [14]:

$$t = \frac{0.9\lambda}{\beta \cos\theta} \tag{4}$$

where 0.9 is the crystalline shape factor,  $\lambda$  is the X-ray wavelength ( $1.54178 \text{ \AA}$ ),  $\beta = (\beta_M^2 - \beta_S^2)^{\frac{1}{2}}$  is the full width at half maximum (FWHM),  $\beta_M$  and  $\beta_S$  are the measured peak broadening and instrumental broadening in radian, respectively, and  $\theta$  is the Bragg angle in radian corresponding to the peak. The dielectric measurement was carried out for the sintered sample using Agilent 4294 A Impedance Analyzer in the frequency and temperature range of 40Hz – 1MHz and 30-400 °C, respectively. The polarization-electric field (P-E) hysteresis characteristics of the samples were determined using a Precision LC material analyzer (Radiant, U.S.A).

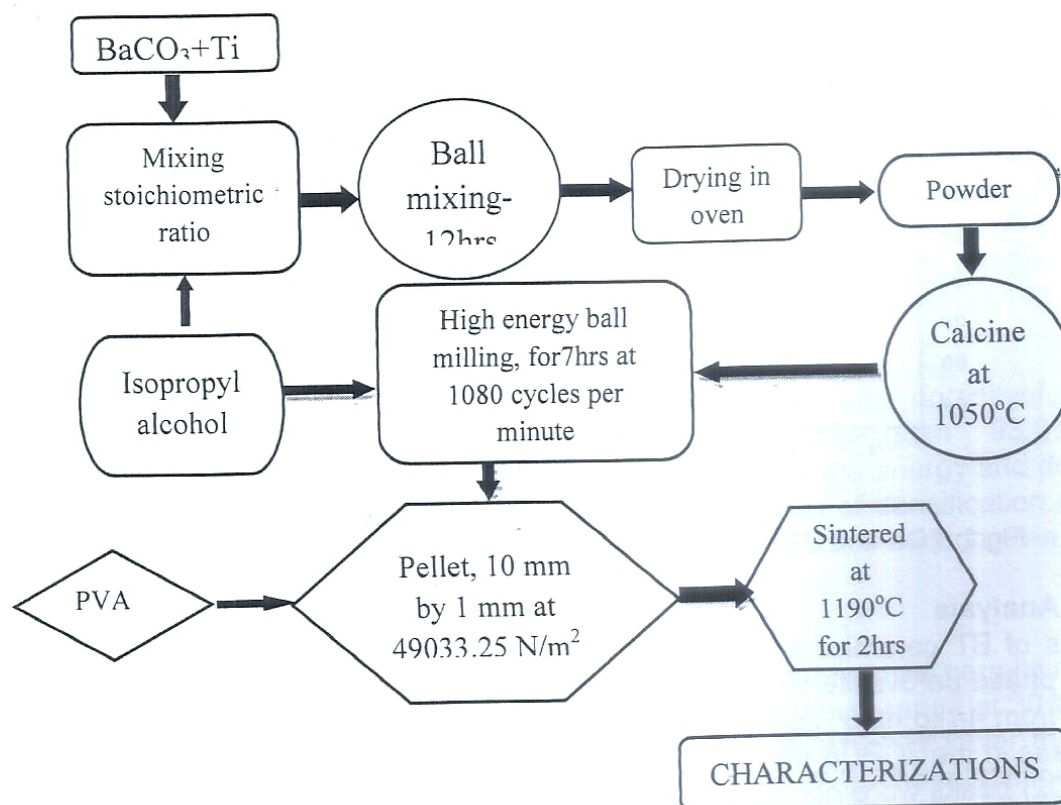


Fig. 1. A Flowchart of the synthesis of BT using a combination of solid state reaction and high-energy ball milling.



### 3.0 Results and discussion

#### 3.1 TG-DSC Analysis

The TG and DSC plots are shown in the Fig.2. Here temperature is taken at X-axis and mass loss (TGA) and heat flow (DSC) in the Y axis. The TGA curve shows total weight loss of 15.51% in two steps. The first step a major weight loss (15.50%) in the temperature range of 602-831°C is attributed to the decomposition of BaCO<sub>3</sub>, similar weight loss is observed by other workers [15]. The second weight loss (0.0047%) in the temperature range of 831-933 is attributed to the formation of BaTiO<sub>3</sub> and the release of CO<sub>2</sub>[16] according to the reaction:



Above 933°C, no substantial weight loss is observed. The weight loss of 15.50% observed experimentally is in agreement with the theoretical weight loss (15.87%) calculated according to the reaction (1).

In the DSC curve, two endothermic peaks have been recorded. The first endothermic peak at ~831°C corresponds to the physical transformation of precursors. The second endothermic peak at ~916°C corresponds to the formation of BaTiO<sub>3</sub> according to chemical equation 1. From DSC curve, the first exothermic at ~940°C is due to the formation of CO<sub>2</sub> molecules [17]. When the temperature is higher than 933°C, the weight of the BaTiO<sub>3</sub> powder no longer decreased, which hints about the calcination temperature of BaTiO<sub>2</sub> to be above 933°C.

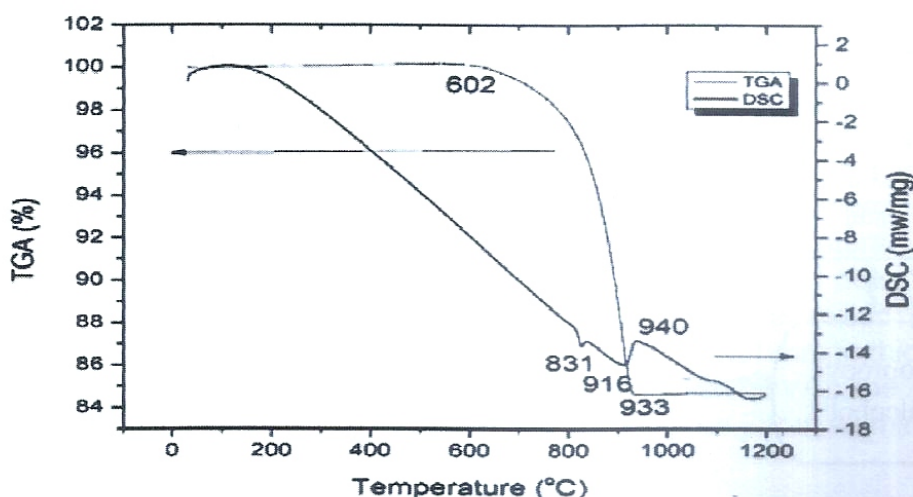
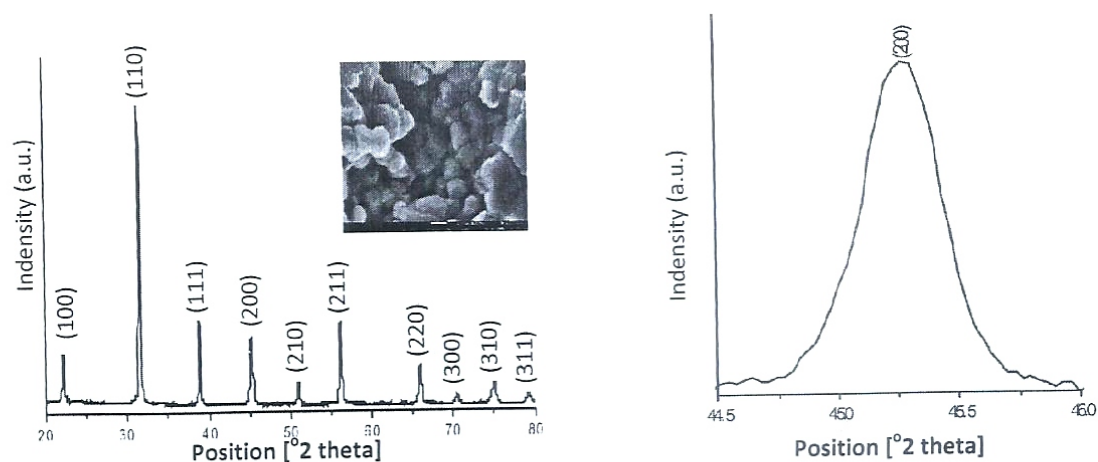


Fig 2. TGA and DSC plot of conventionally heated dried BaTiO<sub>3</sub> powder

#### 3.2 XRD Analysis

XRD patterns of BT ceramics in the range of  $2\theta$  are shown in Fig. 3. The XRD pattern shows cubic phase perovskite structure. The enlarged XRD patterns of the ceramics in the range of  $2\theta$  from 44 to 46.5° clearly show that the crystal structure of BT was assigned to the cubic phase in the JCPDS file no 96-150-7758 and space group  $Pm\bar{3}m$ , because the (200) and (002) peaks were not split [18] as reported by other workers [19, 20]. In general, at room temperature (25-30°C) bulk barium titanate exists in ferroelectric phase, however, due to microstructural size effect nanocrystals of barium titanate are stable in cubic phase [21]. The calculated crystallite size of 31.2 nm for BT is similar to the one of 32 nm obtained by [22]. Lattice constants of BT ceramic were calculated from the XRD spectra to be  $a=b=c=4.0070$  which gives  $c/a$  ratio of 1.000. The crystal cell volumes for and BT were determined to be 64.34 Å<sup>3</sup>.





**Fig. 3. Room temperature XRD Patterns and inset FESEM micrograph at  $\times 100000$  magnification of nanocrystalline BT ceramics sintered at  $1190^{\circ}\text{C}$**

Using the conventional solid-state reaction of  $\text{BaCO}_3\text{-TiO}_2$ , the temperature for synthesizing the BT single phase was higher than  $1200^{\circ}\text{C}$  [23]. Here, the temperature ( $960^{\circ}\text{C}$ ) at which the BT single phase was obtained is significantly lower than that required by the conventional solid-state reaction process. The low formation temperature for BT is believed to be beneficial from the refined powders as a result of HBM [24].

### 3.3 Surface Morphology

The inset of Fig. 3 shows the typical FESEM micrographs of BT ceramics sintered at  $1190^{\circ}\text{C}$  for 2 hrs. It can be seen that the sintered ceramic sample are dense and have varying microstructures with the little presence of voids. The presence of voids in the FESEM images indicate that the pellets have a certain amount of porosity. The grain size and grain boundary are observed very clearly in the non-agglomerated region. The average grain size of BT ceramic is determined by using quadrant technique [25] is  $142.07\text{ nm}$ .

### 3.4 Density and porosity measurement

The calculated theoretical, experimental, relative density and porosity of BT ceramic obtained from equation 1, 2, and 3 are  $6.02\text{ g/cm}^3$ ,  $5.369\text{ g/cm}^3$ ,  $93.6\%$  and  $6.3\%$  respectively. It has been reported that porosity can dissipate the energy and deteriorate the dielectric properties of a material [26]. It indicates the degree of densification of a ceramic. Porosity decreases strength because pores reduce the true cross-section area of a member and also pores act as stress-concentrating notches.

### 3.5 Dielectric properties

Fig. 4 shows the frequency dependence of the real part of relative permittivity ( $\epsilon'$ ) for BT nanocrystalline ceramic sample in the  $40\text{ Hz} - 1\text{ MHz}$  frequency range at  $30$  to  $150^{\circ}\text{C}$ . The highest value of  $\epsilon'$  ( $1600$ ) is obtained at room temperature which is lower than that of the sample prepared by conventional solid state reaction route [27]. The relaxation frequency is about  $3000\text{ Hz}$  for BT at  $90^{\circ}\text{C}$ . It is noted that  $\epsilon'$  decreases with the increase in frequency and temperature as observed by other workers [28]. The decrease of  $\epsilon'$  with increase of frequency arises from the fact that because of inertia, the polarization does not occur instantaneously with the application of the electric field. The delay in response towards the applied alternating electric field leads to decrease in dielectric constant. It is observed that the values of  $\epsilon'$  at all temperatures is higher at low frequencies. This is because at lower



frequencies, all four types' mechanism of polarization (atomic, electronic, dipolar, space charge) contributes to the total polarization of the material. With the increase in frequency, the dipoles with large relaxation times cease to respond with the applied frequency and hence decrease in the dielectric constant is caused. This type of frequency dependence dielectric behavior is found in many ferroelectric materials [29, 30]. A low dispersion of  $\epsilon'$  is observed at 70°C, 110°C, 130°C, and 150°C which becomes frequency independent beyond 100 Hz. At higher frequencies, due to the lack of the ability of dipoles to follow the fast alternation of an applied field, the dielectric constant remains constant [31]. However, the constant arises due to the electronic polarization at higher frequencies. With an increase of the frequency, the ionic and orientation polarizabilities descend, and their contribution finally becomes insignificant.

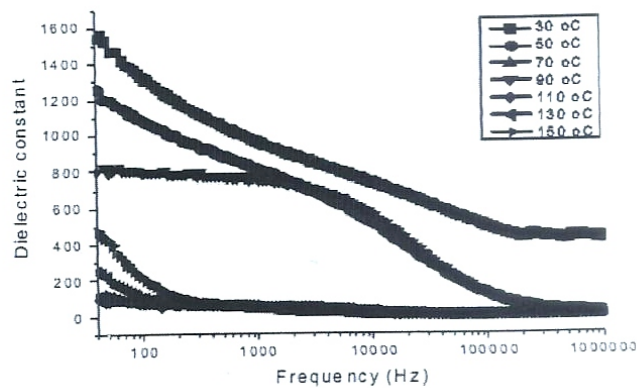


**Fig. 4. Frequency dependences of dielectric constant at various temperature of BT nanocrystalline ceramic.**

Fig. 5 shows the frequency dependences of dielectric loss of nanocrystalline BT ceramic at various temperature. The  $\tan \delta$  of BT shows dispersion at low frequencies with low loss at 30, 50 and 90°C and then decreased sharply with increasing frequency. Thereafter it remains almost constant over the entire frequency range. At 110-150°C, there is dispersion at low frequency with the presence of two relaxation peaks. The peaks observed at low and higher frequency range shift toward high frequency region with increase in temperature, the  $\tan \delta$  decreases with increase in frequency. This indicates the relaxation to be thermally activated [32]. The lowest and highest loss of BT are 0.096 and 1.62 at 90°C and 110°C respectively. Eventually, at all temperature and at higher frequencies, the dielectric losses are reduced, a  $\tan \delta$  is associated with the dissipation of energy in dielectric systems.

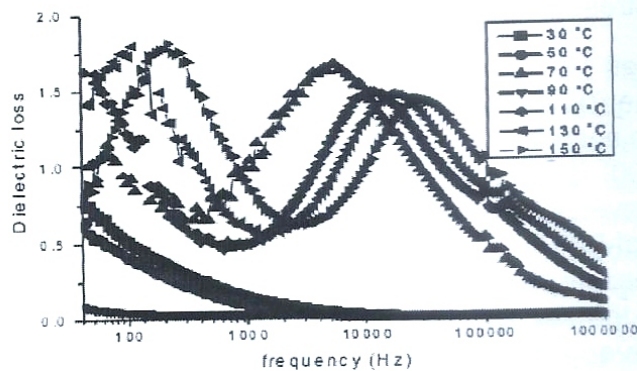


**Fig. 5. Frequency dependences of dielectric loss at room temperature of BT nanocrystalline ceramic**



The variation of the dielectric constant  $\epsilon'$  and dielectric loss ( $\tan \delta$ ) as a function of temperature for nanocrystalline BT ceramic sample measured from room temperature to 150°C at a different frequency is shown in Fig. 6 and 7 respectively. The  $\epsilon'$  at all temperature decrease from 30°C to 70°C and then increases sharply at 90°C and afterward falls to the lowest level at 110°C thus indicating a *ferroelectric–paraelectric phase transition*  $T_c$  at 90°C. It is clear that the  $T_c$  is shifted to a lower value than the one of conventionally sintered BT ( $T_c$  120°C), which is similar to that obtained by others workers [33]. The  $\epsilon'$  peaks at  $T_c$  decrease with increase of frequency (Fig. 5) and is associated to a minimum of the losses (Fig. 6). It is clear that the maximum  $\epsilon'$  of BT is less than the one obtained in CuO-modified BTSZ ceramics synthesized using solid-state method [34]. The low value of the  $\epsilon'$  of BT sintered by HBM should be attributed to two factors, grain size in nanometer range and distortion of crystal lattice caused by HBM. As the grain boundaries increase the grain size decrease and the grain boundary exhibited the polarization of grain boundary may be little or even none. Uchino et al. [19] suggested that with decreasing grain size,  $T_c$  was shifted downward through room temperature, eventually tending toward 0 K at some critical particle size.

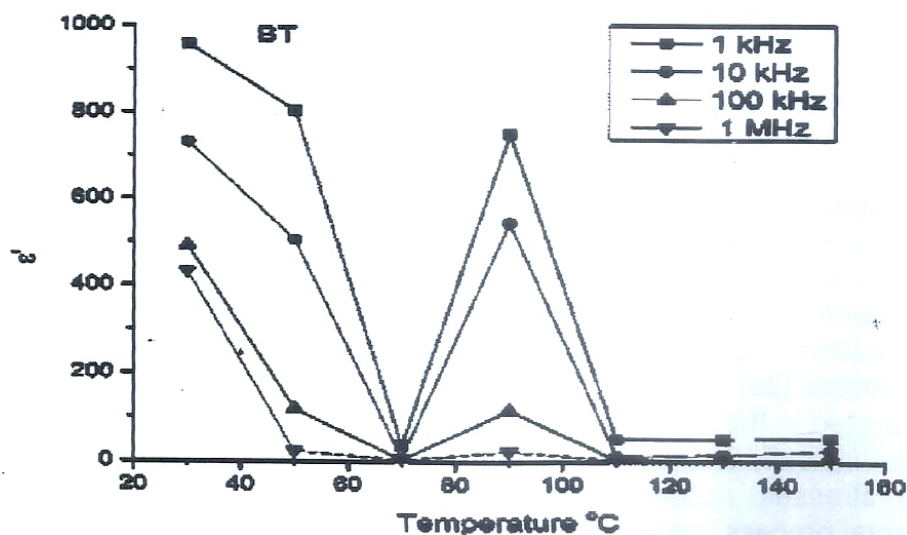


Fig. 6. Temperature dependences of dielectric constant at room temperature of BT nanocrystalline ceramic.

Fig. 7 display the frequency dependence of dielectric loss ( $\tan \delta$ ) of the BT at various frequencies. Similar to the behavior of dielectric constant with frequency, the dielectric loss increases with increasing temperature. This indicates the thermally activated nature of the dielectric relaxation of the system. This sharp increase of dielectric loss in the high-temperature region for BT may be attributed to the increased mobility of charge carriers arising from defects or vacancies in the sample [35]. The maximum  $\epsilon'$  and  $\tan \delta$  obtained at room temperature and  $T_c$  are 957.7, 750.7 and 0.50, 0.048 at 1 kHz respectively.



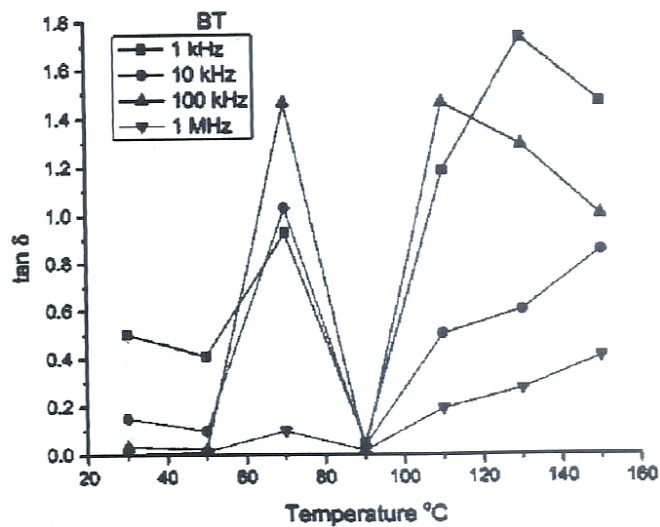


Fig. 7. Temperature dependences of dielectric loss at room temperature of BT nanocrystalline ceramic

### 3.6 Ferroelectric properties

The polarization versus electric field (P-E) hysteresis loops of BT ceramic measured at room temperature and 1 kHz is shown in Fig.8. The values of remanent polarization, coercivity, and saturated polarization are  $0.27 \mu\text{C}/\text{cm}^2$ ,  $581.73 \text{ V}/\text{cm}$ , and  $1.93 \mu\text{C}/\text{cm}^2$  respectively. The polarization hysteresis loop is not fully saturated which might be as a result of leakage current. Residual dipole reorientation causes the difference between maximum polarization at the saturation and the remanent polarization, [17]. The performance parameter of BT is very close to that of the reported value ( $P_s$  of  $2.0 \mu\text{C}/\text{cm}^2$ ) for the ceramic sample [36] and lower than the one obtained having the same composition [37]. It is well reported in the literature that with the decrease in grain size,  $E_c$  increases as each grain is mechanically clamped by its surrounding. This clamping effect, in addition to the mechanical stresses accompanying  $90^\circ$  domain rotations, tends to impede the polarization reversal process, and hence, apparently increases  $E_c$ .

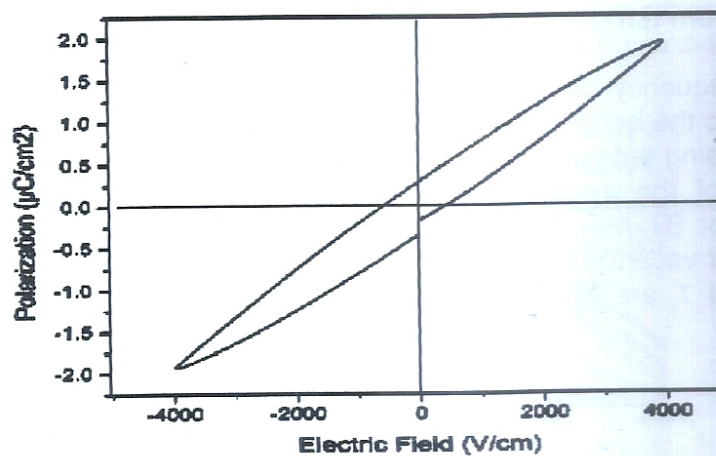


Fig. 8. P-E hysteresis loop of BT nanocrystalline ceramics.



#### 4.0 Conclusion

BT nanocrystalline powder with average crystallite sizes of 31.2 nm and grain size of 142.53 nm was produced by combination of solid state and high-energy ball milling. Thermal analysis of the milled powder confirms that the optimum calcination temperature is 933°C. X-ray analysis shows that the compound has a cubic crystal structure at room temperature. Dielectric properties of sample have been studied in the temperature range between 30 - 150°C and frequency range 40 Hz - 1 MHz. The maximum  $\epsilon'$  and  $\tan \delta$  obtained at room temperature and ferroelectric transition temperature  $T_c$  are 957.7, 750.7 and 0.50, 0.048 at 1 kHz respectively. The remnant polarization ( $P_r$ ) and coercive field ( $E_c$ ) of BT were found to be 0.27  $\mu\text{C}/\text{cm}^2$  and 581.73 V/cm respectively. Therefore, lead-free BT might be useful for multilayer ceramic capacitor and for practical applications.

#### References

- [1]. Stojanovic, B. D., Mastelaro, V.R., Paiva Santos, C. O., and Varela, J. A. (2004). Structure Study of Donor Doped Barium Titanate Prepared From Citrate Solutions. *Science of Sintering*, 36:179-188
- [2] Garbarz, G.B. (2014). Impedance and modulus spectroscopy of a novel ferroelectric ceramics based on barium titanate. *Ferroelectrics* 463; 90e98, doi.org/10.1080/00150193.2014.891924
- [3] Sharma, S., Shamim, K., Ranjan, A., Rai, R., Kumari, P., Sinha, S. (2015). Impedance and Modulus spectroscopy characterization of lead free barium titanate ferroelectric ceramics, *Ceram. Int.* 41, 7713e7722, doi.org/ 10.1016/j.ceramint.2015.02.102
- [4]. Uchino, K. (2000). *Ferroelectric Devices*, Marcel Dekker, New York.
- [5]. Haertling, G. H. (1999). Ferroelectric ceramics: history and technology. *Journal of American Ceramic Society*, 82 (4): 797-818
- [6]. Park, Z.H., Shin, H.S., Lee, B.K., Cho, S.H. (1997). Particle size control of barium titanate prepared from barium titanyloxalate. *Journal of the American Ceramic Society*, 80, 1599–1604.
- [7]. Xu, H., Gao, L., Guo, J. (2002.). Hydrothermal synthesis of tetragonal barium titanate from barium chloride and titanium tetrachloride under moderate conditions. *Journal of the American Ceramic Society*, 85,727–729
- [8]. Pfaff, G. (1992). Sol-gel synthesis of barium titanate powders of various compositions. *Journal of Materials Chemistry*, 2,591–596.
- [9]. Ritter, J.J., Roth, R.S., Blendell, J.E. (1986). Alkoxide precursor synthesis and characterization of phases in the barium-titanium oxide system. *Journal of the American Ceramic Society*, 69,155–162.
- [10]. Tsay, J.D., Fang, T.T. (1996). Effects of temperature and atmosphere on the formation mechanism of barium titanate using the citrate process. *Journal of the American Ceramic Society*, 79, 1693–1696.
- [11]. Milošević, O.B., Mirković, M.K., Uskoković, D.P. (1996). Characteristics and formation mechanism of BaTiO<sub>3</sub> powders prepared by twin-fluid and ultrasonic spray-pyrolysis methods. *Journal of the American Ceramic Society*, 79, 1720–1722.
- [12] Kong, L.B., Zhang, T.S., Ma, J., and Boey, F. (2008). "Progress in synthesis of ferroelectric ceramic materials via high energy mechanochemical technique", *Progress in Material Science*, 53 [2]: 207–322.
- [13] Chandramani, S. K., Natha, A.K., Laishram, R., Thakurb, O.P. (2011). Structural, electrical and piezoelectric properties of nanocrystalline tin-substituted barium titanate ceramics. *J.Alloys. Compd.* 509, 2597
- [14] Scherrer, P. Gottinger Nachricht. (1918). 2, 98
- [15] Padalia, D., Bisht, G., Johri, U.C., Asokan, K. (2013). Fabrication and characterization of cerium doped barium titanate/PMMA nanocomposites. *Solid State Sciences* 19, 122e129
- [16] Jiang, W., Jiang, C., Gong, X., Zhang, Z. (2009). Structure and electrorheological properties of nanoporous BaTiO<sub>3</sub> crystalline powders prepared by sol-gel method. *J Sol-Gel Sci Technol*, 52:8–14 DOI 10.1007/s10971-009-2011-5
- [17] Bera, J., and Sarkar, D. (2003). *J. Electroceramics*, 11[3], 131.
- [18] Buttner, R. H., Maslen, E. N. (1992). *Acta Crystallographica Section B*, 48, 764 - 769,



- [19] Lazarevi, Z.Z., Vijatovi, M.Z., Mitrovi, D.R., Rom, N. Z., Rom, M. J. Rom, N. Paunovi, N., Stojanovi, B.D. (2010). The characterization of the barium titanate ceramic powders Prepared by the Pechini type reaction route and mechanically assisted synthesis. *Journal of the European Ceramic Society* 30, 623–628.
- [20] Yang, X., Li, D., Ren, Z.H., Zeng, R.G., Gong, S.Y., Zhou, D.K., Tian, H., Li, J.X., Xu, G., Shen, Z.J., and Hana, G.R. (2016). Colossal dielectric performance of pure barium titanate ceramics consolidated by spark plasma sintering. *RSC Adv.*, 6, 75422 DOI: 10.1039/c6ra14741k
- [21] Uchino, K., Sadanaga, E., Hirose, T. (1989). *J. American Ceramic Society*.72, 1555–1558.
- [22] Rath, M.K., Pradhan, G.K., Pandey, B., Verma, H.C., Roul, B.K., and Anand, S. (2008). Synthesis, characterization and dielectric properties of europium-doped barium titanate nanopowders. *Materials Letters*, 62, 2136–2139
- [23] Beauger, J., Mutin, C., and Niepce, J. C. (1983). *J. Mater. Sci.* 18, 3543-3550.
- [24] Kong, T.S., Zhang, Ma, J., and Boey, F. (2008). *Prog.Mater. Sci.* 53, 207-322.
- [25] Abrams, H. (1971). Grain size measurement by the intercept method. *Metallography, Volume 4, Issue 1*, February 1971, Pages 59-78. [https://doi.org/10.1016/0026-0800\(71\)90005-X](https://doi.org/10.1016/0026-0800(71)90005-X)
- [26] Shao, S. F., Zhang, J. L., Zhang, Z., Zheng, P., Zhao, M. L., Li, J. C., and Wang, C. L. (2008). *Journal of Physics and Dielectric: Applied Physics*. 41:125408.
- [27] Ganguly, P. Jha, A.K. (2010). *Journal of Alloys and Compound*. 495, 7–12.
- [28] Yang, J., Deng, X., Li, J., Cai, Q., Zhang, H., Wang, L., Su, K., Zhang, G., and Wang, C. (2013). Broadband Dielectric Spectroscopy Analysis of Dielectric Properties of Barium Titanate Ceramics. *Advanced Materials Research* Vol.744, pp 323-328, doi: 10.4028/www.scientific.net/AMR.744.323
- [29] Sinclair, D.C., and West, A.R. (1989). "Impedance and modulus spectroscopy of semiconducting BaTiO<sub>3</sub> showing positive temperature coefficient of resistance," *Journal of Applied Physics*, vol. 66, pp. 3850-3856.
- [30] Sinclair, D.C., and West, A.R. (1994). "Effect of atmosphere on the PTCR properties of BaTiO<sub>3</sub> ceramics," *Journal of Materials Science*, vol.29, pp.6061-6068.
- [31] Kumar, P., and Kar, M. (2014). Effect of structural transition on magnetic and optical properties of Ca and Ti co-substituted BiFeO<sub>3</sub> ceramics. *Journal of Alloys and Compound*. 584 566
- [32] Kumari, K., Prasad, A., Prasad, K. (2016). Dielectric, Impedance/Modulus and Conductivity Studies on [Bi<sub>0.5</sub>(Na<sub>1-x</sub>K<sub>x</sub>)<sub>0.5</sub>]<sub>0.94</sub>Ba<sub>0.06</sub>TiO<sub>3</sub>, (0.16 ≤ x ≤ 0.20) Lead-free Ceramics. *American Journal of Materials Science*, 6(1): 1-18, DOI: 10.5923/j.materials.20160601.01
- [33] Al-Nabulus, T., Bolos, M., Tenailleau, C., Dufour, P., Zakhour, M. (2016). Elaboration and characterization of barium titanate powders obtained by the mechanical activation of barium nitrate and titanate oxide, and electrical properties of the ceramics sintered by SPS. *Journal of ceramic processing research/International Organization for Ceramic Processing*, Hanyang University Press, 17(8), pp.870-875.
- [34] Damjanovic, D. (2005). *The science of Hysteresis*, Volume 3; I. Mayergoyz and G. Brtotti (Eds.) Chapter 4, pg. 337, Elsevier
- [35] Deshpande, S. B., Potdar, H. S., Patil, M. M., Deshpande, V. V., and Khollam, Y. B. (2006). Dielectric Properties of BaTiO<sub>3</sub> Ceramics Prepared from Powders with Bimodal Distribution. *J. Ind. Eng. Chem*, Vol 12, No. 4, 584-588.
- [36] Takeuchi, H. Jyomura, S., Yamamoto, E. and Ito, Y. (1982). *J. Acoust. Soc. Am.* 72(4)1114
- [37] Zong, W. L. (2000). *Ferroelectric Physics*. Beijing: Science publishing press.